






















TESS Hunt for Young and Maturing Exoplanets (THYME) XII: A Young Mini-Neptune on the Upper Edge of the Radius Valley in the Hyades Cluster

ADAM DISTLER ¹, MELINDA SOARES-FURTADO ^{1,2,*}, ANDREW VANDERBURG ², JACK SCHULTE ³,
JULIETTE BECKER ¹, ANDREW W. MANN ⁴, STEVE B. HOWELL ⁵, ADAM L. KRAUS ⁶, KHALID BARKAOU ^{7,8,9},
CÉSAR BRICEÑO ¹⁰, KAREN A. COLLINS ¹¹, DENNIS CONTI ¹², JON M. JENKINS ⁵, MARY ANNE LIMBACH ¹³,
SAMUEL N. QUINN ¹¹, RICHARD P. SCHWARZ ¹¹, SARA SEAGER ^{2,8,14}, JAKE D. TURNER ¹⁵,
JOSEPH D. TWICKEN ^{16,5}, JOSHUA N. WINN ¹⁷ AND CARL ZIEGLER ¹⁸

¹Department of Astronomy, University of Wisconsin-Madison, 475 N. Charter St., Madison, WI 53706, USA

²Department of Physics and Kavli Institute for Astrophysics and Space Research, Massachusetts Institute of Technology, Cambridge, MA 02139, USA

³Center for Data Intensive and Time Domain Astronomy, Department of Physics and Astronomy, Michigan State University, East Lansing, MI 48824, USA

⁴Department of Physics & Astronomy, The University of North Carolina at Chapel Hill, Chapel Hill, NC 27599-3255, USA

⁵NASA Ames Research Center, Moffett Field, CA 94035, USA

⁶Department of Astronomy, The University of Texas at Austin, Austin, TX 78712, USA

⁷Astrobiology Research Unit, Université de Liège, Allée du 6 Août 19C, B-4000 Liège, Belgium

⁸Department of Earth, Atmospheric and Planetary Sciences, Massachusetts Institute of Technology, Cambridge, MA 02139, USA

⁹Instituto de Astrofísica de Canarias (IAC), Calle Vía Láctea s/n, 38200, La Laguna, Tenerife, Spain

¹⁰Cerro Tololo Inter-American Observatory, Casilla 603, La Serena, Chile

¹¹Center for Astrophysics | Harvard & Smithsonian, 60 Garden Street, Cambridge, MA 02138, USA

¹²American Association of Variable Star Observers (AAVSO), 185 Alewife Brook Parkway, Suite 410, Cambridge, MA 02138 USA

¹³Department of Astronomy, University of Michigan, Ann Arbor, MI 48109, USA

¹⁴Department of Aeronautics and Astronautics, MIT, 77 Massachusetts Avenue, Cambridge, MA 02139, USA

¹⁵Department of Astronomy and Carl Sagan Institute, Cornell University, Ithaca, NY, USA

¹⁶SETI Institute, Mountain View, CA 94043, USA

¹⁷Department of Astrophysical Sciences, Princeton University, Princeton, NJ 08544, USA

¹⁸Department of Physics, Engineering and Astronomy, Stephen F. Austin State University, 1936 North St, Nacogdoches, TX 75962, USA

ABSTRACT

We present the discovery and characterization of TOI-4364 b, a young mini-Neptune in the tidal tails of the Hyades cluster, identified through *TESS* transit observations and ground-based follow-up photometry. The planet orbits a bright M dwarf ($K = 9.1$ mag) at a distance of 44 pc, with an orbital period of 5.42 days and an equilibrium temperature of 488^{+4}_{-4} K. The host star's well-constrained age of 710 Myr makes TOI-4364 b an exceptional target for studying early planetary evolution around low-mass stars. We determined a planetary radius of $2.01^{+0.10}_{-0.08} R_{\oplus}$, indicating that this planet is situated near the upper edge of the radius valley. This suggests that the planet retains a modest H/He envelope. As a result, TOI-4364 b provides a unique opportunity to explore the transition between rocky super-Earths and gas-rich mini-Neptunes at the early stages of evolution. Its radius, which may still evolve as a result of ongoing atmospheric cooling, contraction, and photoevaporation, further enhances its significance for understanding planetary development. Furthermore, TOI-4364 b's moderately high Transmission Spectroscopy Metric of 44.2 positions it as a viable candidate for atmospheric characterization with instruments such as JWST. This target has the potential to offer crucial insights into atmospheric retention and loss in young planetary systems.

Keywords: exoplanets, star clusters, planets and satellites: individual (TOI-4364)

1. INTRODUCTION

Investigations of young exoplanets offer crucial insights into the rapid evolutionary changes that occur within the first few hundred million years after the for-

mation of a planet. During this early period, planets undergo significant transformations in their orbital dynamics (e.g., Chambers & Wetherill 1998; Adams & Laughlin 2006; Morbidelli et al. 2012), structural properties (Kite et al. 2009), as well as atmospheric composition and structure (e.g., Owen & Wu 2017; Dorn et al. 2018; Ginzburg et al. 2018).

To investigate these early evolutionary processes, the *TESS* Hunt for Young and Maturing Exoplanets (THYME; Newton et al. 2019) collaboration focuses on detecting and characterizing transiting exoplanets within young stellar groups and open clusters. These environments are advantageous because the ages, distances, and metallicities of the stars are well-constrained, enabling more accurate exoplanetary and host star parameters. Consequently, the young exoplanets identified by THYME and similar surveys serve as key benchmarks for testing theories of exoplanet formation, migration, and evolution.

The nearby Hyades cluster, located at a distance of 46 pc and estimated to be ≈ 700 Myr old (Brandner et al. 2023), is an ideal target for this search. In this work, we present the discovery, characterization, and follow-up observations of a planet in the tidal tails of the Hyades cluster. This planet, TOI-4364 b, is the eighth detected in the cluster, joining K2-25 b (Mann et al. 2016), K2-136 b/c/d (Ciardi et al. 2018; Mann et al. 2018), HD 283869 b (Vanderburg et al. 2018), HD 285507 b (Quinn et al. 2014), and HD 28305 b (Sato et al. 2007). Although membership in the Hyades has been questioned for HD 28305 (Taberner et al. 2012; Röser et al. 2019) and HD 283869 (Douglas et al. 2014; Oh & Evans 2020; Long et al. 2023), we include these stars as Hyades members in the figures presented in this work.

TOI-4364 b is found in this work to be a transiting mini-Neptune with a 5.42-day orbit around an M dwarf. With a radius of $2.01^{+0.10}_{-0.08} R_{\oplus}$, this planet resides at the upper edge of the radius valley (Fulton et al. 2017a), a region where planets with radii between $1.5 - 2.0 R_{\oplus}$ are scarce. Typically, planets smaller than the lower bound are rocky, while those larger than the upper bound are gaseous mini-Neptunes. Some of the most widely accepted mechanisms proposed to drive the formation of the radius valley are photoevaporation (Owen & Wu 2017; Burn et al. 2024) and core-powered mass loss (Ginzburg et al. 2018).

The youth and K -band brightness ($K = 9.1$ mag) of this newly discovered planetary system make it a compelling target for follow-up observations. As a young mini-Neptune on the upper edge of the radius valley, TOI-4364 b provides a unique opportunity to explore atmospheric properties and the processes shaping planetary evolution, with its bright, young M dwarf host offering valuable insights into atmospheric retention and loss during the early stages of planetary formation.

Table 1. *TESS* Photometry Used in the Detection and Characterization of TOI-4364 b.

<i>TESS</i> Data Overview				
Sector	Cadence	Camera	CCD	Observation Dates
5	120 s	1	2	2018 Nov 11 – Dec 06
32	120 s	1	2	2020 Nov 20 – Dec 15

The manuscript is structured as follows: §2 details the data products used for the detection and characterization of this system; §3 focuses on the characterization of stellar properties of TOI-4364, along with the analysis of TOI-4364 b and its orbit; §4 examines potential false positive scenarios, §5 discusses TOI-4364 b in the context of other Hyades planets and within the broader census of exoplanet discoveries.

2. DATA

To investigate potential planetary transits of the Hyades star TOI-4364, we used photometric data from the Transiting Exoplanet Survey Satellite (*TESS*; Ricker et al. 2015), photometry and radial velocity (RV) measurements from ground-based facilities, and high-resolution speckle imaging.

2.1. The TOI-4364 *TESS* Light Curve

The *TESS* survey divides the sky into rectangular sectors. Each sector covers a field of view of $24^{\circ} \times 96^{\circ}$ over a baseline of approximately 26 days. To date, TOI-4364 (TIC 4070275) has been observed in Sector 5 and Sector 32 (start dates: 11/11/2018 & 11/20/2020). The data are available with a time sampling of 120 seconds. Table 1 lists the relevant sectors, cadence, camera number, CCD number, and date range corresponding to these observations.

The data from both sectors were reduced and analyzed by the Science Processing Operations Center (SPOC) at NASA Ames Research Center (Jenkins et al. 2016). On May 27, 2021, SPOC conducted a transit search of the combined light curve from the two sectors, using an adaptive, noise-compensating matched filter (Jenkins 2002; Jenkins et al. 2010, 2020). This resulted in a Threshold Crossing Event with 5.42 d period. An initial limb-darkened transit model was fitted (Li et al. 2019) and a suite of diagnostic tests were performed to help assess the planetary nature of the signal (Twicken et al. 2018). The transit signature passed all diagnostic tests presented in the SPOC Data Validation reports, and the source of the transit signal was localized within $1.23 \pm 3.61''$ of the target star. The *TESS* Science Office (TSO) reviewed the vetting information and issued an alert for TOI 4364.01 on August 5, 2021.

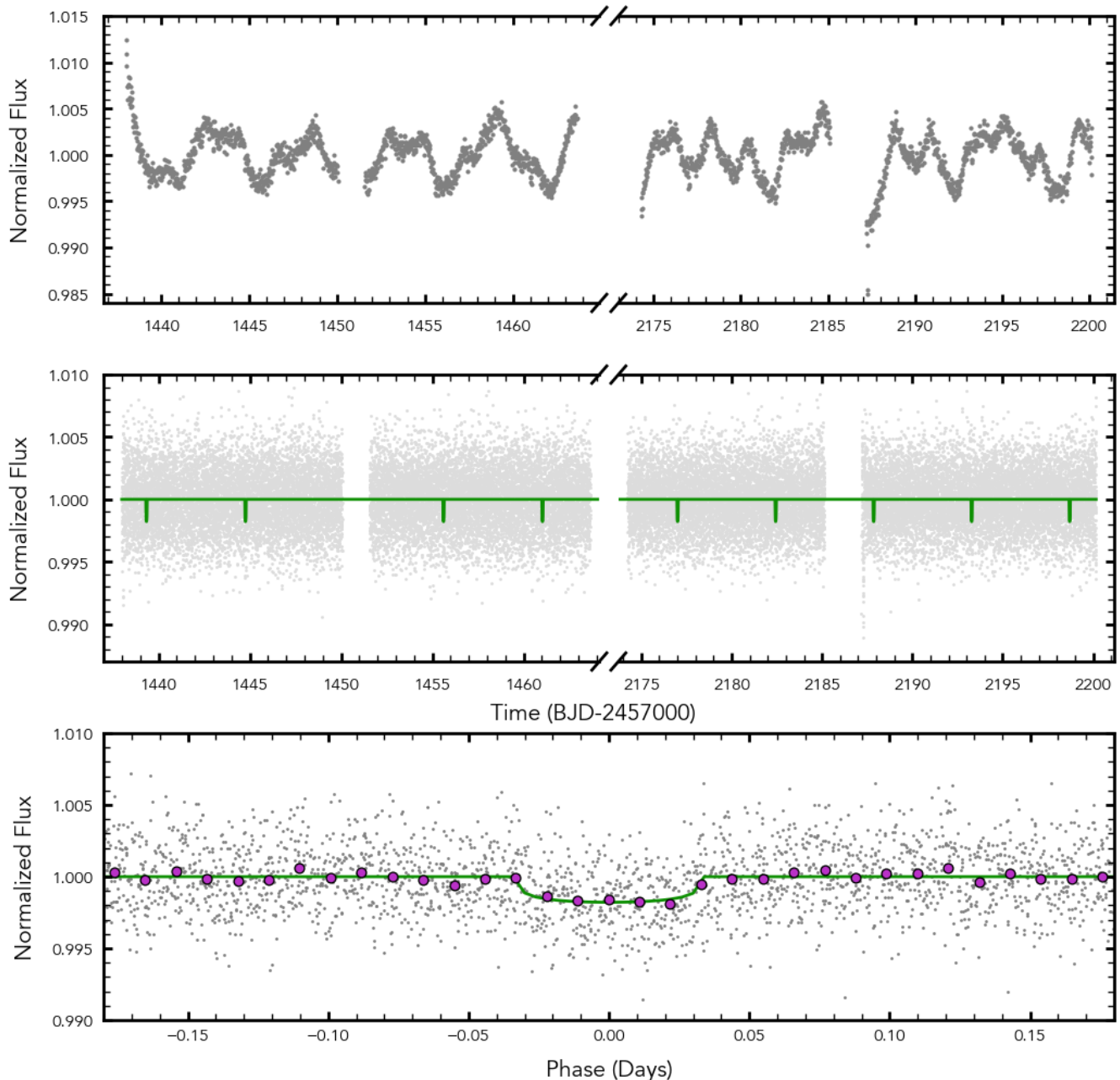


Figure 1. *TESS* light curve analysis for TOI-4364 b. **Top:** unflattened, processed light curve of TOI-4364. **Middle:** flattened, systematically-corrected light curve (grey) with the best fit *batman* (green). **Bottom:** phase-folded light curve with binned points (purple) and the phase-folded best-fit transit model (green).

For young, active stars, specialized processing can significantly mitigate *TESS* light curve noise. We performed additional systematic correction to the SPOC simple aperture photometry light curve (Twicken et al. 2010; Morris et al. 2020) using the method outlined by Vanderburg et al. (2019). This approach involved simultaneously fitting a basis spline with 0.3-day intervals to model the low-frequency stellar variability, along with several vectors describing spacecraft systematics. These

vectors included the mean and standard deviation of the quaternion time series to correct for pointing jitter.

We also incorporated cotrending vectors from SPOC’s band 3 correction to address fast timescale variations (Smith et al. 2012; Stumpe et al. 2012, 2014) and included a 0.1-d high-pass filtered version of the background flux time series in the decorrelation. We performed a linear least-squares fit to the light curve and removed the contributions of the systematics vectors to produce a cleaned light curve. We then removed the

high-frequency stellar variability by subtracting a basis spline fit at 0.5-day breakpoints.

Following these corrections, we searched the light curve for box-shaped dips in brightness using the box-least-squares (BLS) algorithm (Kovács et al. 2002), investigating a period range of 0.4–26 days. A compelling 5.42-day signal was apparent at a statistical significance of 11.95, calculated following the method of Kipping (2023). The processed data along with a phase-folded light curve are shown in Figure 1.

In addition, we explored the existing transit signals using the Transit Least Squares¹ (TLS) algorithm (Hippke & Heller 2019). By incorporating considerations such as limb darkening effects with transit ingress and egress, the TLS algorithm can more accurately model transit shapes, leading to improved detection efficiency. Using the TLS algorithm, we again recovered the transit signal with the same ephemeris. We attribute the observed periodic signal to the detection of a new planet candidate, TOI-4364 b, with a transit depth of approximately 2 ppt. This is consistent with the transit depth expected from a mini-Neptune companion.

2.2. Ground-based Seeing-Limited Photometry

Follow-up observations using instruments with smaller pixel plate scales can help determine the source of a potential planetary signal. This is important given the large pixel plate scale of *TESS*. Moreover, planetary transit parameters can be refined by reducing third-light contamination (see Ciardi et al. 2015) and the ephemeris can be more accurately constrained. Follow-up photometric observations were conducted using several 1.0-meter telescopes from the Las Cumbres Observatory Global Telescope (LCOGT; Brown et al. (2013)) Network — a worldwide array of robotic telescopes designed for continuous sky monitoring. Each telescope is equipped with Sinistro cameras, optimized for high-precision photometry. Observations were made at four sites: the South African Astronomical Observatory (SAAO), the Cerro Tololo Inter-American Observatory (CTIO), the Siding Spring Observatory (SSO), and the Teide Observatory. The details of these observations are summarized in Table 2.

Over six months, seven observing sessions were carried out, with six capturing the full transit and one focusing on the planet’s egress. All observations were performed using the *i*’ filter, ensuring consistent data quality across sites. The science data reduction was performed using the standard LCOGT BANZAI pipeline (McCully et al. 2018a). Photometric measurements were extracted using uncontaminated apertures, ranging between 4.0–6.6”, using the *AstroImageJ*² software (Collins et al. 2017). These small apertures were chosen to exclude

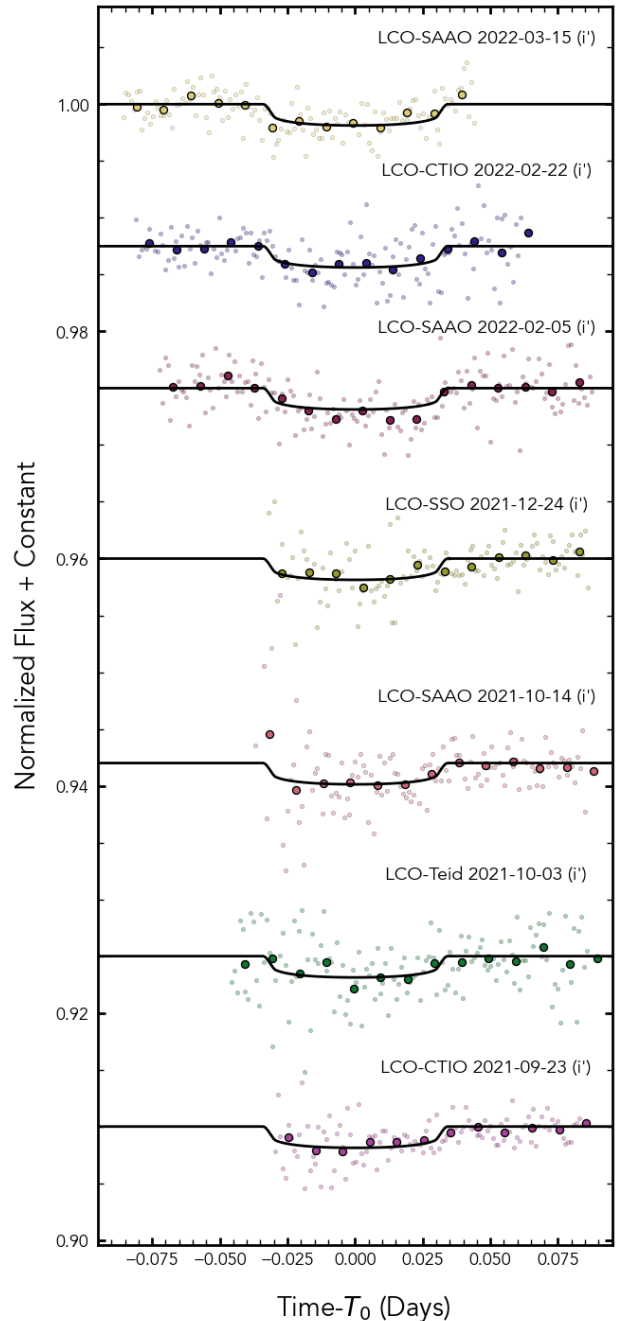


Figure 2. LCOGT 1-m TOI-4364 b follow-up observations (small points) along with binned data (larger circles) and best-fit transit models (black line). Individual observations are shifted along the y-axis for clarity.

contamination from a nearby ($\sim 11''$) neighbor that was present in the SPOC apertures. *Gaia* DR3 identified no contaminating sources brighter than $G_{\text{Gaia}} > 21$ mag closer than this neighbor. The transits were detected convincingly in six of the seven follow-up observations taken, with the data shown in Figure 2.

¹ <https://transitleastsquares.readthedocs.io>

² <https://www.astro.louisville.edu/software/astroimagej>

Table 2. Follow-up ground-based photometry of TOI-4364 b.

Las Cumbres Observatory Global Telescope Network				
Location	Duration	Coverage	Aperture	Date
SAAO ^a	191 min	Full	5.4"	03/15/2022
CTIO ^b	208 min	Full	5.1"	02/22/2022
SAAO	234 min	Full	5.1"	02/05/2022
SSO ^c	174 min	Full	5.1"	12/24/2021
SAAO	177 min	Full	4.0"	10/14/2021
Teide	189 min	Full	5.0"	10/03/2021
CTIO	165 min	Egress	6.6"	09/23/2021

^aSouth African Astronomical Observatory

^bCerro Tololo Inter-American Observatory

^cSiding Spring Observatory

2.3. Radial Velocity Measurements

Several ground-based RV measurements have been collected for our target, along with *Gaia* DR3 spectra (Gaia Collaboration et al. 2021a). The ground-based spectroscopic follow-up consists of four measurements with the Echelle SPectrograph for Rocky Exoplanets and Stable Spectroscopic Observations (*ESPRESSO*) (Pepe et al. 2021), which span over three months. It also includes two measurements with the Tillinghast Reflector Echelle Spectrograph (*TRES*; Szentgyorgyi & Fűrész 2007; Fűrész 2008), which are separated by three days.

The *ESPRESSO* data were reduced with the Data Reduction Software (DRS) pipeline, which cross-correlates the observed spectrum with a stellar binary mask, and then fits the cross-correlation output with a Gaussian to derive the RV. The *TRES* data were first reduced following the method in Buchhave et al. (2010). A CCF multi-order analysis was then applied to the data to best constrain the RV across the entire spectrum. The precise and stable measurements from *TRES* and *ESPRESSO* help to distinguish between planetary signals and potential perturbations caused by unseen stellar companions, with all measurements taken at or near quadrature. We see that the standard deviation of the *ESPRESSO* data is 9.0 m s^{-1} , and the *TRES* data are separated by 78 m s^{-1} . When we convert the measurements from the two spectrographs to the standard IAU velocity scale, we find that they match at the 220 m s^{-1} level. All of this is consistent with TOI-4364 not being a short-period radial velocity variable. The details of these observations are listed in Table 3.

2.4. High Resolution Speckle Imaging

To investigate potential contamination from stars at small angular separations (possible variables, eclipsing

Table 3. Radial Velocity Measurements of TOI-4364.

Name	RV	err	Exp. time	Time
	(km s^{-1})	(km s^{-1})	(s)	
<i>Gaia</i> DR3 ^a	44.77	0.46	–	2016.0
<i>TRES</i>	44.969	0.104	2160	2459522.907
<i>TRES</i>	44.980	0.104	2400	2459525.825
<i>ESPRESSO</i>	45.087	0.004	1800	2459795.889
<i>ESPRESSO</i>	45.108	0.001	1800	2459812.881
<i>ESPRESSO</i>	45.103	0.003	1800	2459813.828
<i>ESPRESSO</i>	45.109	0.002	1800	2459893.824

^a*Gaia* DR3 RV measurements are averaged over multiple visits over 34 months with an average of 8 transits per star.

binaries, or bound companions), we performed high-resolution speckle imaging. By analyzing the speckle data, we can investigate whether the observed transits are influenced by additional “third-light” from close stellar companions. This ensures that the planetary signal remains free from contamination by additional stellar light, which is crucial for accurate characterization and validation of the planet (Furlan & Howell 2017, 2020).

The first Gemini speckle observation for TOI-4364 occurred on October 16, 2021, and was made with the ‘Alopeke instrument on Gemini North in Hawaii. The second Gemini observation took place on Gemini South in Chile on January 5, 2023, using the Zorro instrument under conditions of better seeing and offering more time on target. The two instruments are identical, using Electron Multiplying Charge-Coupled Devices (EMCCDs) to enable fast readout and provide simultaneous two-color imaging (Scott et al. 2021). Both observations of TOI-4364 were performed using narrow band filters at two separate wavelengths, 832/40 nm and 562/54 nm. This dual-wavelength approach provides a more comprehensive assessment of any detected nearby sources. The speckle data was reduced using our standard pipeline described in Howell et al. (2011). No sources were detected to our magnitude limits, as shown in the top panel of Figure 5.

On October 18, 2021, a broader search for stellar companions was conducted using speckle imaging with the 4.1-meter Southern Astrophysical Research (SOAR) telescope (Tokovinin 2018). The observation was made in the Cousins *I*-band (879 (289) nm), a visible band-pass similar to *TESS*. Further details about these observations can be found in the SOAR *TESS* survey (Ziegler et al. 2020). No nearby stars were detected within $3''$ of TOI-4364 in the SOAR observations, as shown in the bottom panel of Figure 5. Beyond the outer limits of these observations, the *Gaia* DR3 catalog estab-

lishes that there are no neighbors brighter than $G_{\text{Gaia}} \approx 21$ mag and within $10''$. Further, a search of *Gaia* DR3 finds that there are no very wide co-moving, co-distant companions brighter than this magnitude limit out to a projected separation of $1200''$ (50,000 AU). Therefore, the system does not host any wide binary companions that might induce long-term dynamical evolution of the planetary system.

3. ANALYSIS

To optimally characterize the star-planet system, we leveraged the properties that TOI-4364 shares with the Hyades to then perform a global analysis of the star-planet system.

3.1. Association of TOI-4364 with the Hyades Cluster

Galactic space velocity values were calculated using `PyAstronomy` tools, following the methodology outlined in Johnson & Soderblom (1987) and utilizing data from *Gaia* DR3. The spatial center of the Hyades cluster is $(-44.77, +0.40, -16.24)$ pc (Röser et al. 2019). This can be compared to the Cartesian Galactic coordinates of TOI-4364, measured as $(-36.47, -17.86, -16.56)$ pc. TOI-4364 is approximately 20.1 pc from the core of the Hyades cluster. It has been shown that the Hyades exhibits a dispersed structure, including extensive tidal tails that span over one hundred parsecs in size (Röser et al. 2019). The structure of the cluster has been studied in detail using 3D kinematic modeling, confirming that TOI-4364 is a high-confidence member of the Hyades, with a membership probability exceeding 99% (Oh & Evans 2020). The location of TOI-4364 within the tidal tail (Röser et al. 2019) accounts for its distance relative to the core members of the Hyades (Lodieu et al. 2019).

3.2. TOI-4364 Photometric Rotation Period

To accurately determine the photometric rotation period of TOI-4364, we analyzed the processed *TESS* data, as described in §2. The data were binned to 30 minutes to reduce scatter, better capturing longer-period stellar rotation signals. We also removed contaminated parts of the light curve, which included the initial 0.2 days of Sector 5 and the first 0.2 days after the downlink of Sector 32.

Our Lomb-Scargle (LS) periodogram (Lomb 1976; Scargle 1982) and autocorrelation function (ACF) analysis suggested a photometric rotation rate of approximately 5 days. However, under more scrutiny, we observed recurring substructure in the light curve indicating a ~ 10 day rotation period. This recurring substructure is illustrated in the top left and right panels of Figure 3.

To optimally characterize this structure, we employed a phase dispersion minimization (PDM) algorithm from the package `starrotate`. The PDM algorithm detects periodic signals in unevenly sampled data by folding

it over trial periods and minimizing the scatter within phase bins (described further in Stellingwerf (1978)). The θ value reflects the scatter on the folded data, with values closer to zero having less scatter, with values closer to one having more scatter.

The photometric rotation period is dependent upon the presence of spots, spot latitude, and the strength of differential surface rotation. We measured a period of 10.51 days for Sector 5 and 10.63 days for Sector 32. The PDM output and corresponding phase-folded light curves are shown in Figure 3.

Stellar rotation offers a method to estimate a cluster’s age. Skumanich (1972) showed that average stellar rotational velocity decreases with cluster age. For low-mass stars, this decline is driven by magnetic braking, where the star’s magnetic field interacts with outflowing charged particles, removing angular momentum and slowing rotation over time (Mestel 1968; Gossage et al. 2023).

Consequently, the rotational sequence of a cluster can be compared with those of other clusters to estimate its age. Figure 4 illustrates the rotation sequence for the Hyades alongside the Pleiades (120 Myr), Praesepe (670 Myr), and NGC 6811 (1 Gyr). The rotational sequence of the Hyades exhibits a slope comparable to that of Praesepe (Gossage et al. 2018), thus supporting our age estimate of 710 ± 100 Myr. Note that M dwarfs, like our planet host TOI-4364, exhibit a wide dispersion of rotation periods.

3.3. EXOFASTv2 Analysis

To determine the best-fit transit parameters, our team constructed a global fit from the EXOFASTv2³ (Eastman et al. (2013); Eastman et al. (2019)) software package. EXOFASTv2 utilizes a differential evolution Markov Chain Monte Carlo (MCMC) approach to fit both planetary and stellar parameters within a system simultaneously. This allowed us to jointly model the star’s spectral energy distribution (SED) using PARSEC (Bressan et al. 2012) in parallel with *TESS* and follow-up transit observations of the planet, thereby ensuring consistency across the data.

To construct the SED, we gathered archival photometric data from several sources: *Gaia* DR3 (Gaia Collaboration et al. 2016, 2021b), the Two Micron All Sky Survey (2MASS; Cutri et al. (2003)), and the Wide-field Infrared Survey Explorer (WISE; Wright et al. 2010; Cutri & et al. 2012). To set an upper bound for the visual extinction, we used the Bayestar 3D dust maps (Green et al. 2015; Green 2018; Green et al. 2019) and we calculated a value of $A_V = 0$. To account for this in the EXOFASTv2 analysis, we then set an upper bound of $A_V < 0.001$. In regard to previous estimates for the Hyades (see Brandner et al. (2023) for a sum-

³ <https://github.com/jdeast/EXOFASTv2>

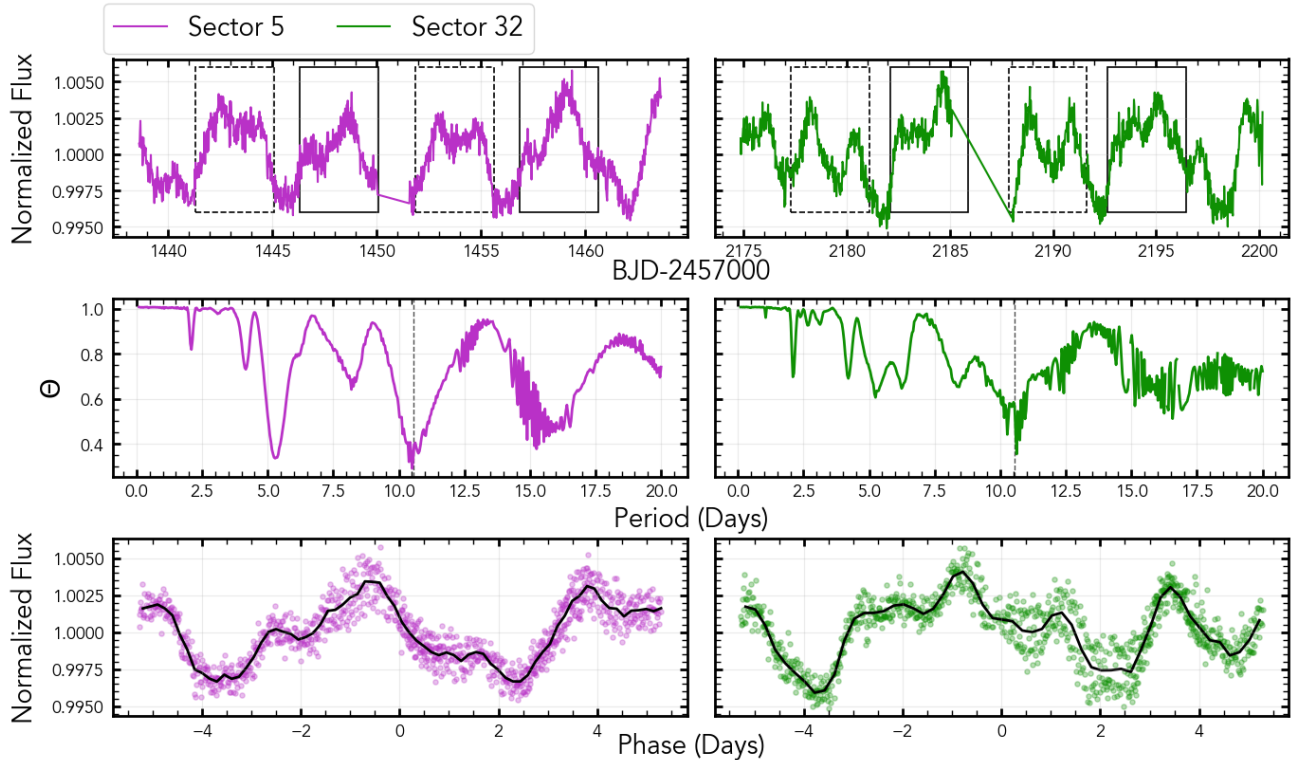


Figure 3. Analysis of TOI-4364’s photometric rotation period using *TESS* Sectors 5 (purple) and 32 (green). **Top:** Trimmed light curve with boxes showing similar structures; **Center:** PSM output, with maximum likely periods shown with dashed lines; **Bottom:** Phase-folded light curves for each sector at $P = 10.57$ days.

mary), we opted to adopt a broad Gaussian prior for the age of TOI-4364 of 700 ± 100 Myr and a metallicity of $[\text{Fe}/\text{H}] = 0.155 \pm 0.095$ dex.

The planetary parameters are predominately constrained by the transit light curves listed in Tables 1-2. The *TESS* light curves were processed using the method discussed in §2.1. They were then flattened using `keplersplinev2`,⁴ a Python-based spline fitting tool. The spline breakpoint spacing was chosen as the value that minimizes the Bayesian Information Criterion (BIC). The *TESS* light curves were then truncated to remove unnecessary out-of-transit data, retaining a baseline of one transit duration on either side of each transit. The follow-up light curves were flattened using `AstroImageJ` (Collins et al. 2017). No prior estimate was placed on the linear and quadratic limb darkening coefficients, which were allowed to vary as free parameters. To estimate the mass of the planet, `EXOFASTv2` uses the mass-radius relation from Chen & Kipping (2017).

We followed the default `EXOFASTv2` MCMC setup, with twice as many chains as the number of parameters in each fit. For the circular fit, this meant 46 parameters and 92 chains. For the fit where eccentricity was allowed to float, there were 50 parameters and 100 chains. To en-

sure robust and converged results, we implemented strict convergence criteria, requiring a Gelman-Rubin statistic (Gelman & Rubin 1992) less than 1.01 and more than 1000 independent draws. The Gelman-Rubin statistic criterion is typically the more difficult to reach. In the case of the eccentric fit, the MCMC had a Gelman-Rubin statistic of 1.0084 and 5783 independent draws after accepting 9.26% of the total number of steps. Our `EXOFASTv2` MCMC circular fit resulted in a Gelman-Rubin statistic of 1.0041 and 4727 independent draws after accepting 17.02% of the total number of steps. The resulting stellar parameters are provided in Table 4. The orbital fit parameters are provided in Table 5. The best-fit models are illustrated in Figures 1-2.

4. RULING OUT FALSE POSITIVE SCENARIOS

4.1. Possible False Positive Scenarios

In our efforts to validate the detection of TOI-4364 b, we utilized `LEO-vetter`,⁵ an automated tool designed to assess potential exoplanet signals in light curve data. TOI-4364 b successfully passed all assessments conducted by `LEO-vetter`, including flux and pixel vetting analyses. These tests examined the transit shape to

⁴ <https://github.com/avanderburg/keplersplinev2>

⁵ <https://ascl.net/2404.026>

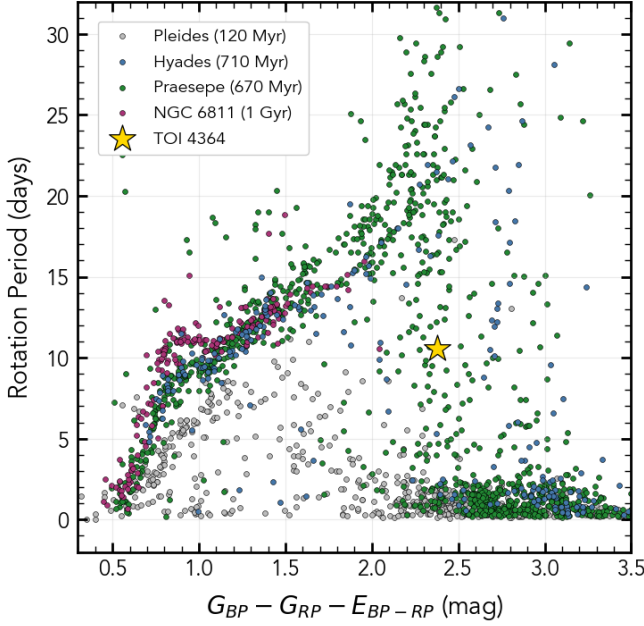


Figure 4. The color-rotation sequence for catalog members of the Hyades cluster, as compared to the Pleiades (120 Myr; Rebull et al. 2016), Praesepe (670 Myr; Douglas et al. 2017), and NGC 6811 (1 Gyr; Curtis et al. 2019). TOI-4364 is depicted as a gold star.

exclude eclipsing binaries and analyzed centroid offsets to confirm the accuracy of the transit event locations.

Given the absence of additional validation methods for TOI-4364 b, we worked to exclude all plausible false positive scenarios, as detailed below.

- Instrumental Artifacts and Stellar Variability:** No instrumental artifacts in the TOI-4364 *TESS* light curves have been identified that could replicate the observed signal in the BLS periodogram. Furthermore, the transit signal has been independently verified photometrically by observations from four separate facilities, eliminating the likelihood of an instrumental artifact. While M-dwarfs are known for their significant variability (Mignon et al. 2023), particularly those younger than 1 Gyr, no known phenomenon could induce a transit-like flux dip that recurs consistently over multiple years. Stellar variability typically manifests as gradual changes over days, weeks, or months, rather than the distinct transit-like flux dips observed.
- Target is an Eclipsing Binary:** A possible concern is that the target star might be an eclipsing binary (EB). However, if this were the case, one would expect large-scale RV variations on the order of kilometers per second, as the companion would need to have an inclination of near 90 degrees to produce a transit-like signal. Instead, the

Parameter	Value	Source
TIC ID	4070275	<i>TESS</i> Input Catalog
<i>Gaia</i> DR3 ID	3210444215030339584	<i>Gaia</i> DR3
Astrometry		
α .	80.067 ± 0.014	<i>Gaia</i> DR3
δ .	-4.239 ± 0.011	<i>Gaia</i> DR3
μ_α (mas yr ⁻¹)	64.456 ± 0.017	<i>Gaia</i> DR3
μ_δ (mas yr ⁻¹)	43.789 ± 0.014	<i>Gaia</i> DR3
π (mas)	22.805 ± 0.012	<i>Gaia</i> DR3
distance (pc)	43.85 ± 0.04	<i>Gaia</i> DR3
Photometry		
Spectral Type	M4V	This paper
G_{Gaia} (mag)	12.534 ± 0.006	<i>Gaia</i> DR3
G_{BP} (mag)	13.796 ± 0.033	<i>Gaia</i> DR3
G_{RP} (mag)	11.420 ± 0.012	<i>Gaia</i> DR3
V (mag)	13.56 ± 0.03	Zacharias et al. (2013)
J (mag)	9.952 ± 0.024	2MASS
H (mag)	9.307 ± 0.022	2MASS
Ks (mag)	9.075 ± 0.024	2MASS
W1 (mag)	8.949 ± 0.023	ALLWISE
W2 (mag)	8.857 ± 0.02	ALLWISE
W3 (mag)	8.764 ± 0.03	ALLWISE
W4 (mag)	8.833 ± 0.438	ALLWISE
A_V (mag)	0.00050 ± 0.00034	This paper*
Kinematics & Galactic Position		
RV_{Bary} (km s ⁻¹)	44.770 ± 0.455	<i>Gaia</i> DR3
U (km s ⁻¹)	-43.505 ± 0.047	This paper
V (km s ⁻¹)	-19.235 ± 0.018	This paper
W (km s ⁻¹)	-2.002 ± 0.015	This paper
X (pc)	-36.469 ± 0.039	This paper
Y (pc)	-17.855 ± 0.016	This paper
Z (pc)	-16.555 ± 0.003	This paper
Physical Properties		
P_{rot} (days)	10.57 ± 0.06	This paper
Age (Myr)	710 ± 100	This paper
T_{eff} (K)	3528^{+33}_{-20}	This paper
M_\star (M_\odot)	$0.487^{+0.017}_{-0.016}$	This paper*
R_\star (R_\odot)	$0.4684^{+0.0087}_{-0.010}$	This paper*
L_\star (L_\odot)	$0.03075^{+0.00085}_{-0.00084}$	This paper*
L_X (erg s ⁻¹)	2.07×10^{28}	Freund et al. (2020)
ρ_\star (g cm ⁻³)	$6.69^{+0.38}_{-0.33}$	This paper*
$\log(g)$ (log(cm/s ²))	$4.785^{+0.017}_{-0.016}$	This paper*
[Fe/H] (dex)	0.148 ± 0.046	This paper*

Table 4. Stellar properties of TOI-4364. Values marked with an asterisk were obtained from EXOFASTv2.

TRES data reveals a maximum spread between RVs to be 78 ms^{-1} (taken at opposite quadratures), indicating that TOI-4364 is not an EB in a 5.42 day orbit.

- Contamination by Foreground or Background Eclipsing Binaries:** Another potential false positive scenario is the presence of an EB in the foreground or background of the target, which would not have an effect on the RV measurements of TOI-4364. Given the large pixel scale of *TESS*, this is an important consideration.

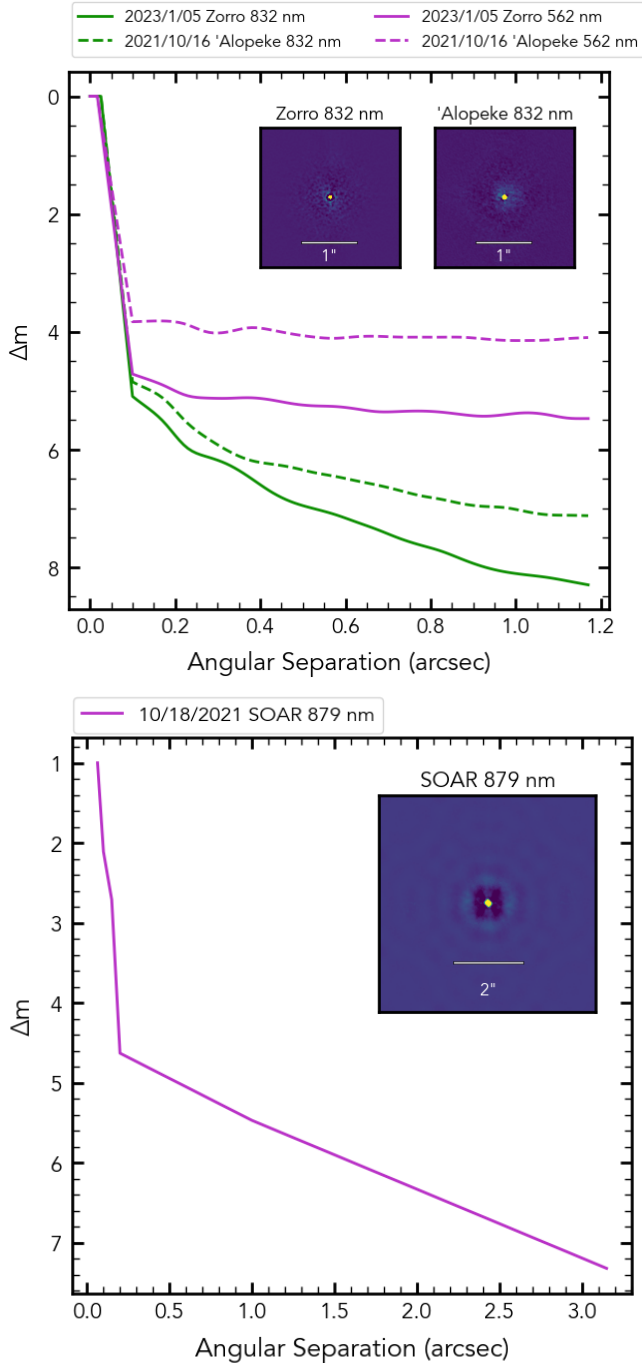


Figure 5. Top Panel: Contrast curves obtained from Gemini North ‘Alopeke and Gemini South Zorro instruments. Insets showcase 832 nm reconstructed images, highlighting the increased contrasts achieved with Zorro on Gemini South due to better seeing conditions and a longer total integration time. No close companion star was detected within the achieved 5σ magnitude contrast curves and angular limits from the 8-m diffraction limit out to $1.2''$. At the distance of TOI-4364, these limits correspond to spatial separations ranging from $0.88 - 52.8$ AU. **Bottom Panel:** SOAR sensitivity curve taken on October 18, 2021. The 5σ sensitivity limits are shown out to $3.15''$, corresponding to a projected separation of 138.1 AU.

Parameter	Value e free	Value $e = 0$
P (days)	$5.424019^{+0.000010}_{-0.000011}$	5.424019 ± 0.000011
T_0 (BJD)	2458439.3428 ± 0.0020	2458439.3431 ± 0.0020
a/R_*	$21.83^{+0.41}_{-0.36}$	$21.86^{+0.41}_{-0.36}$
i (degrees)	$88.68^{+0.85}_{-0.40}$	$88.46^{+0.11}_{-0.10}$
e	$0.29^{+0.38}_{-0.17}$	0
ω_* (degrees)	-190^{+160}_{-130}	0
u_1 (TESS)	0.312 ± 0.036	0.287 ± 0.036
u_2 (TESS)	0.34 ± 0.036	$0.360^{+0.036}_{-0.035}$
u_1 (i')	0.341 ± 0.021	$0.316^{+0.019}_{-0.020}$
u_2 (i')	$0.315^{+0.020}_{-0.021}$	0.336 ± 0.019
R_p/R_*	$0.0394^{+0.0017}_{-0.0014}$	$0.0402^{+0.0012}_{-0.0013}$
δ_{TESS}	0.00178 ± 0.00010	0.00175 ± 0.00010
$\delta_{i'}$	0.00179 ± 0.00010	0.00180 ± 0.00010
t_{14} (days)	$0.0668^{+0.0020}_{-0.0015}$	$0.0677^{+0.0014}_{-0.0013}$
t_{12} (days)	$0.00298^{+0.0013}_{-0.00047}$	$0.00393^{+0.00023}_{-0.00022}$
Derived Parameters		
R_p (R_\oplus)	$2.01^{+0.10}_{-0.08} R_\oplus$	$2.05^{+0.08}_{-0.08}$
a (AU)	$0.04753^{+0.00053}_{-0.00054}$	0.04753 ± 0.00053
T_{eq} (K)	488^{+4}_{-4}	534.4 ± 3.9
TSM	44.2	45.1
ESM	4.9	5.1

Table 5. Transit-Fit Parameters for TOI-4364 b. **Top:** Transit fits obtained from the joint SED, TESS, and follow-up photometry using the EXOFASTv2 model. **Bottom:** Derived system parameters. The middle column presents the results when the eccentricity (e) and argument of periapsis (ω) are allowed to vary as free parameters. The rightmost column shows the fit assuming $e = 0$ and $\omega = 0$.

The required magnitude difference of a contaminating EB is given by

$$\Delta m \lesssim 2.5 \log_{10} \left(\frac{t_{12}^2}{t_{13}^2 \delta} \right), \quad (1)$$

where δ is the transit depth, t_{12} is the ingress duration, t_{14} is the full transit duration, and $t_{13} = t_{14} - t_{12}$ (Vanderburg et al. 2019).

To calculate this magnitude difference, our team employed the differential MCMC code `edmc`⁶ coupled with `batman`⁷ to optimally constrain the orbital parameters. We employed the data, as described in §2.1, removing observations that were not within ± 0.1 days of the transit (as predicted by EXOFASTv2). We ran the code with 50 walkers for 10,000 links, with 4,000 burn-in links. We fixed the eccentricity to zero and argument of periapsis to 90° and used a prior of the EXOFASTv2 output for the walkers. All orbital parameters were run to a Gelman-Rubin statistic of < 1.05 . Following this analysis, we arrive at a limiting contaminating EB

⁶ <https://github.com/avanderburg/edmc>

⁷ <https://lkreidberg.github.io/batman/docs/html/index.html>

magnitude of $\Delta m \leq 3.65$ mag at 95% confidence. The Zorro 832 nm speckle imaging contrast curves in Figure 5 illustrate a 3.87 mag contrast at $0.085''$, corresponding to a projected separation of 3.73 AU. For the outer limit, the 879 nm *SOAR* imaging observation (bottom panel of Figure 5) also confirmed the lack of an object bright enough to cause this signal out to $3''$. Although this is within the follow-up photometric radius, a 15.04 *TESS* magnitude star would be clearly resolved by *Gaia* given a contrast sensitivity above 99% for $\Delta G_{\text{Gaia}} < 6$ mag (Brandeker & Cataldi 2019). Given that the follow-up photometry constrained the signal to be within $4.0''$ of TOI-4364, it is very unlikely the signal comes from a contaminating EB.

- **Physically Associated Eclipsing Binaries:** Another possibility is that TOI-4364 has a physically associated EB companion that could account for the observed signal. This cannot be completely ruled out, as the angular separation may be small enough such that it is unresolved by the speckle imaging. In such a case, the inclination would need to be near-zero degrees to prevent a significant RV shift in TOI-4364. This is unlikely for several reasons. Firstly, it is statistically unlikely given that M dwarfs have a very low triple rate of $\approx 3.3\%$ (Winters et al. 2019). Secondly, the Zorro contrast curve rules out the presence of companions bright enough to induce this signal at distances beyond 3.73 AU (corresponding to a maximum period of 10.3 years). Given the maximum of *ESPRESSO* RV shift of 28 m s^{-1} shift (taken over three months), a companion would need to have an extremely low inclination. While there is no way to completely rule out this scenario, it is unlikely that a bound EB is producing the transit signal of TOI-4364 b.

4.2. Statistical Validation with *TRICERATOPS*

To further validate our conclusion that no false positive scenarios could mimic the signal of TOI-4364 b, we employed the *TRICERATOPS* pipeline (Giacalone et al. 2021) to assess the likelihood of various false positive scenarios. *TRICERATOPS* utilizes Bayesian inference to compute the probability that an input light curve originates from a wide range of scenarios. This includes assessing the shape of the transit signature and conducting checks for instrumental artifacts or background contamination.

We ran *TRICERATOPS* twenty times using data from the contrast curves obtained by the Zorro speckle imaging. Each run included 10^6 instances, which yielded a false positive probability — the likelihood that the transit signal is not due to a planet — of 0.00319 ± 0.00017 . Similarly, the nearby false positive probability — the

likelihood that the transit signal is due to a nearby object — was found to be 0.00317 ± 0.00017 . These low false alarm probabilities allow us to statistically confirm that TOI-4364 b is indeed a planet. Moreover, while the false alarm probabilities are low, they likely overestimate the true values since existing follow-up photometry using smaller apertures could not be included. From this analysis, we conclude that TOI-4364 b is a genuine exoplanet.

5. DISCUSSION

5.1. TOI-4364 b in Context

TOI-4364 b serves as a key benchmark for studying exoplanets within the Hyades cluster, which is known to host eight planets. Table 6 presents a comparison of TOI-4364 b’s properties with those of the other Hyades planets. Notably, TOI-4364 b has the second shortest orbital period among them. Short-period planets like in clusters are important follow-up targets, amenable to further constraints and characterization. Further, its location near the upper boundary of the radius valley makes it a particularly valuable target for probing planetary evolution. Given its youth and proximity, TOI-4364 b offers an invaluable opportunity to investigate how planetary radii evolve as a function of system age.

Table 6. Planets in the Hyades

Planet	Period (d)	Radius (R_{\oplus})	Distance (pc)
TOI-4364 b	5.4	2.0	43.9
K2-25 b	3.5	3.4	45.0
HD 285507 b	6.1	13.8	45.0
K2-136 b	8.0	1.0	59.2
K2-136 c	17.3	2.9	59.2
K2-136 d	25.6	1.5	59.2
HD 283869 b	106.0	2.0	47.5
HD 28305 b	594.9	–	44.7

When compared to the broader population of confirmed exoplanets, as shown in Figure 6, TOI-4364 b continues to stand out for its proximity to Earth. This is especially significant when considering planets younger than 1 Gyr with well-constrained ages. For clarity, we define a “well-constrained” age as one where both the upper and lower error is at most 20% of the estimated value. The apparent brightness of TOI-4364 b make it an exceptional target for studying planetary evolution among M dwarf planetary companions. Precise age constraints for M dwarf planets are often lacking due to the host stars’ low luminosity and the challenges associated with dating these slowly-evolving stars. The proximity of TOI-4364 b, combined with its well-constrained age, provides a rare opportunity to address this gap, offering critical insights into how planets form, migrate, and evolve around low-mass stars.

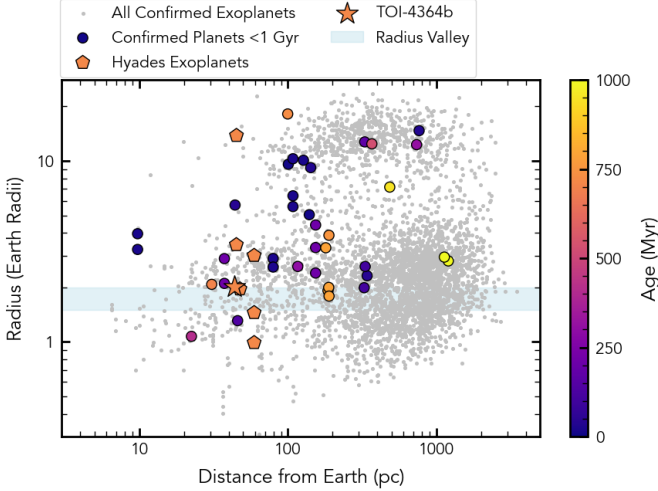


Figure 6. Distance from Earth versus planet radius for confirmed exoplanets (grey circles), young (< 1 Gyr) planets with well-constrained ages (colored circles), previously discovered Hyades exoplanets (pentagons), and TOI-4364 b (star). TOI-4364 b stands out as a nearby young planet at the upper edge of the radius valley, making it a prime target for atmospheric and evolutionary studies.

Figure 7 illustrates the period-radius diagram, highlighting young objects with precisely measured age estimates, including TOI-4364 b and other known Hyades exoplanets. Even among young systems, TOI-4364 b currently resides at a critical boundary of the radius valley.

5.2. Evolving Physical and Orbital Properties

Comparisons to older planets and broader planet samples must be contextualized with the ongoing evolutionary changes that are relevant to a young planet like TOI-4364 b. In the following subsections, we discuss some of these considerations.

5.2.1. Planetary Radius

The measured radius of TOI-4364 b of $2.01^{+0.10}_{-0.08} R_{\oplus}$ places it just above the threshold where a planet is expected to possess an H/He envelope (Lopez & Fortney 2014; Rogers 2015). Yet, given the young age of this planet, it is important to note that the radius is likely to change with time, due to both cooling and photoevaporation from the insolation by the host star. Younger planets will retain higher levels of envelope entropy, and as planets with H/He envelopes are irradiated by their host stars, they will also lose mass due to photoevaporation. This mass loss rate (Watson et al. 1981; Lopez et al. 2012; Luger & Barnes 2015; Barnes et al. 2020) can be modeled as:

$$\dot{m} = \epsilon \left(\frac{R_p^3 L_{\text{XUV}}}{4K a^2 G M_p} \right), \quad (2)$$

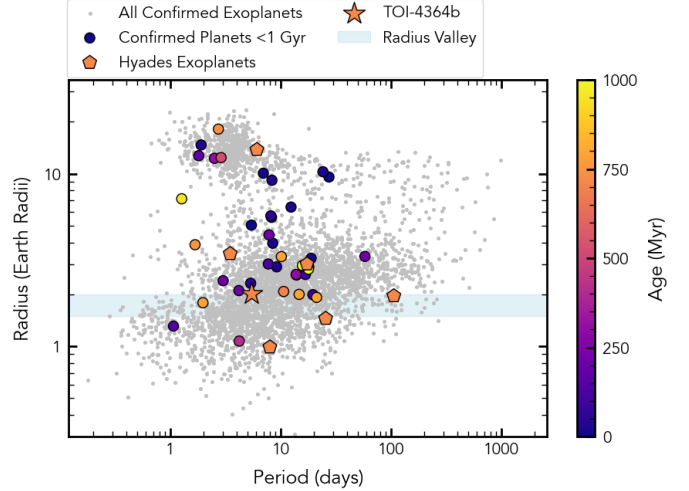


Figure 7. Period-radius distribution of confirmed exoplanets (grey circles), confirmed young (< 1 Gyr) exoplanets with well-constrained ages (colored circles), previously discovered Hyades exoplanets (pentagons), and TOI-4364 b (star). To enhance the readability of the figure, we omit planets discovered via direct imaging. Note that TOI-4364 b resides at the upper edge of the radius valley (blue strip).

where $\epsilon = 0.1$ is the heating efficiency, R_p is the radius of the planet, L_{XUV} is the XUV luminosity of the host star, K is the tidal enhancement factor (Erkaev et al. 2007), a is the semi-major axis, G is the gravitational constant, and M_p is the mass of the planet (predicted from Chen & Kipping 2017 to be $5.3^{+1.9}_{-1.2} M_{\oplus}$). We assume that the planetary atmosphere becomes optically thick to XUV photons at $1 R_p$. In the subsequent analysis, we set all planetary parameters to be their best-fit values given in Table 5 for the free-eccentricity solution, and assume a stellar mass of $0.49 M_{\odot}$.

To evaluate the radius evolution of TOI-4364 b, we ran a series of models using the code VPlanet (Barnes et al. 2020) and its AtmEsc and STELLAR modules. VPlanet allows us to integrate the effects of photoevaporation and planetary cooling to simulate the evolution of a planet’s radius as a function of stellar age, planet mass, and envelope fraction. In our models, we use interpolated stellar luminosity tracks from Baraffe et al. (2015) and the mass-radius model from Lopez et al. (2012). Our simulations assume that photoevaporation begins after disk dissipation at approximately 10 Myr.

In the first set of simulations, we set the planet mass to the predicted mass from Chen & Kipping 2017, running 300 simulations with initial H/He envelope mass fraction varying between 0% – 10%. The results of these simulations are shown in Figure 8, which depicts the computed evolution for each of our 300 grid points. For comparison to the models, the current-day measured radius of TOI-4364 b is denoted by a red point with error bars denoting the 1σ uncertainty. Models consistent with the

observed radius of TOI-4364 b are denoted by darker, thicker lines, with the nominal best-fit solution shown by the largest line width. Models consistent with the observed radius at 710 Myr, correspond to current H/He envelope fraction ranging between 0.4% – 0.9%. This corresponds to an initial H/He envelope mass fraction range of 0.8% – 1.4%. The best-fit solution suggests an initial envelope fraction of 1.0%, which, after accounting for the aforementioned evolutionary processes, results in a current H/He envelope fraction of 0.6%. Over the next few Gyr, the predicted radius evolution for these allowed solutions is minimal, with a maximal 10% decrease.

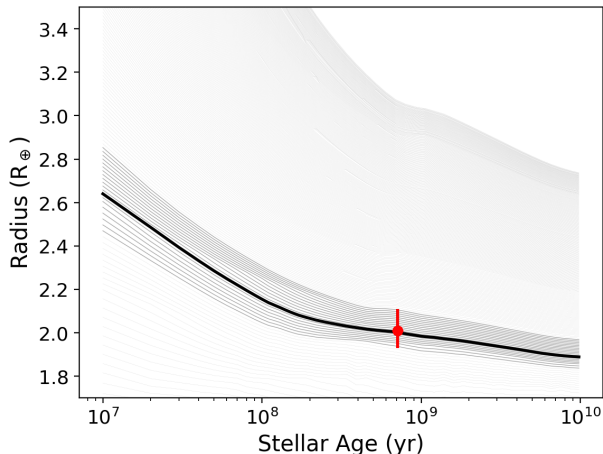


Figure 8. Evolution of the planetary radius as a function of stellar age for TOI-4364 b, assuming the best-fit planetary parameters (including planetary mass). The grey and black lines represent the radius evolution predicted by the `VPLanet` model, which incorporates both planetary cooling and photoevaporation effects. Each line corresponds to a different initial H/He envelope fraction, ranging from 0% – 10%. The red point marks the observed planetary radius at 710 Myr, with error bars indicating the 1σ uncertainty. The darker contour lines show models that are consistent with the observed radius, which have H/He envelope fractions between 0.4% – 0.9%. The nominal best-fit solution is shown as a thicker line, which corresponds to a current-day envelope fraction of 0.6%. Over time, the planet’s radius is expected to decrease gradually due to continued cooling and mass loss from photoevaporation.

We ran a second set of simulations to assess the impact of the uncertainty of the planetary mass on the computed allowable envelope fractions. In the second set of simulations, we varied both the planet’s mass (within the 1σ range) and its initial envelope fraction, with a total of 20 grid points in each dimension for a total of 400 simulations. This resulted in a broader range of viable initial H/He envelope mass fractions. These span between 0.5% – 1.8%, with current envelope mass fractions ranging between 0.4% – 1%. In this case, the

predicted radius evolution is more substantial, with the planet’s radius potentially decreasing by up to 15% over the next few Gyr. We note that these envelope fractions assume the planet’s true mass lies within the 1σ range given by [Chen & Kipping 2017](#).

5.2.2. Tidal Locking

Understanding whether TOI-4364 b is tidally locked to its host star is crucial for accurate interpretation of the planet’s atmospheric circulation patterns, atmospheric evolution (including the presence of enhanced atmospheric stripping), and thermal evolution. More specifically, when tidal forces synchronize a planet’s rotation to the frequency of its orbit, the day side of the planet receives *all* of the incident radiation, which directly impacts the aforementioned atmospheric properties (e.g., [Pierrehumbert & Hammond 2019](#); [Grießmeier et al. 2004](#)).

For short-period planets, tidal forces will tend to lock the planetary spin frequency to the planetary mean motion on a timescale given by

$$t_{lock} \approx \frac{\omega a^6 I Q}{3GM_\star^2 k_2 R_p^5}, \quad (3)$$

where ω is the planet’s initial rotation rate, I is the moment of inertia of the planet, Q is the planet’s tidal dissipation factor (a dimensionless number that describes how efficiently tidal energy is dissipated within the planet), and M_\star is the mass of the host star, k_2 planet’s Love number (which characterizes how much the planet deforms in response to tidal forces) ([Gladman et al. 1996](#)).

Instead of solving for the tidal locking time by assuming Q , one can provide an age constraint and determine the minimum Q required for the system to not be locked. Assuming an initial rotation rate of one cycle per Earth day, a $Q \gtrsim 10^8$ is required to tidally lock the planet within 710 Myr. All the Solar System planets have values much lower than this, including Uranus and Neptune ($Q \approx 10^5$, [Tittlemore & Wisdom 1990](#)). Similarly, terrestrial planets have values much lower than this ($Q \approx 10 - 300$, [Goldreich & Soter 1966](#)). As such, we can reasonably conclude that this planet is tidally locked.

5.3. Metrics for Atmospheric Characterization

Characterizing a planet’s atmosphere is crucial for understanding its composition and structure. Two key metrics used to assess exoplanet atmospheres — particularly in preparation for observations with next-generation telescopes like the James Webb Space Telescope (JWST) — are the Transmission Spectroscopy Metric (TSM) and the Emission Spectroscopy Metric (ESM). These metrics help prioritize targets for detailed follow-up studies based on the planet’s ability to reveal atmospheric properties through transit and emission observations.

A fundamental parameter influencing both the TSM and ESM is the planet’s equilibrium temperature, which provides a baseline for estimating atmospheric thermal structure and potential for atmospheric escape. For TOI-4364 b, this temperature gives valuable insight into the energy balance of the planet and its atmospheric stability. By calculating these metrics, we can assess TOI-4364 b’s value as a target for transmission and emission spectroscopic follow-up. Assuming an albedo (α) of 0.3, and perfect heat redistribution, the equilibrium temperature is approximated by

$$T_{\text{eq}} = \left(\frac{L_{\star}(1 - \alpha)}{16\pi\sigma a^2} \right)^{\frac{1}{4}}, \quad (4)$$

where L_{\star} is the host star’s luminosity and σ is the Stefan-Boltzmann constant. We calculate an equilibrium temperature of 488^{+4}_{-4} K for TOI-4364 b.

The TSM evaluates the planet’s suitability for transmission spectroscopy, where the atmosphere is observed as the planet passes in front of its host star, as defined in [Kempton et al. \(2018\)](#). For TOI-4364 b, we derive a TSM of 44.2, indicating that this is a modest candidate for transmission observations when compared to the most promising TSM targets. Yet, this value is particularly compelling when compared to the values of other young systems with well-constrained ages, as described in §5.4.2.

The ESM, which is also defined in [Kempton et al. \(2018\)](#), measures the planet’s suitability for emission spectroscopy — the detection of thermal radiation from the planet’s dayside when illuminated by its star. Using the formula from [Cowan & Agol \(2011\)](#) for a tidally locked planet, the dayside temperature is given by

$$T_{\text{day}} = \left[\frac{2}{3}(1 - \alpha) \right]^{\frac{1}{4}} T_{\text{sub}}, \quad (5)$$

where T_{sub} represents the temperature at the substellar point (the point on the planet’s surface such that the host star is at the zenith) and is given by

$$T_{\text{sub}} = T_{\text{eff}} \left(\frac{R_{\star}}{a} \right)^{\frac{1}{2}}, \quad (6)$$

where R_{\star} is the stellar radius. For TOI-4364 b, we derive an ESM of 4.9, also indicating this is a viable candidate for emission observations. Once again, this is a particularly compelling target when compared to values of other young, well-constrained systems, as described in §5.4.2.

5.4. Future Work Characterizing TOI-4364 b

5.4.1. Radial Velocity Observations

To accurately determine the mass of TOI-4364 b, high-precision RV measurements are essential. Assuming

a planetary mass of $5.3^{+1.9}_{-1.2} M_{\oplus}$ from [Chen & Kipping \(2017\)](#), we would expect an RV semi-amplitude of $3.55^{+1.3}_{-0.93} \text{ m s}^{-1}$. Contemporary high-precision spectrographs, such as WIYN/NEID, ESPRESSO, the Habitable Zone Planet Finder, and Gemini/MaroonX have the technological capability of detecting RV variations of this magnitude. However, a young M dwarf is expected to have high amplitude stellar variability, potentially posing challenges for obtaining a mass measurement.

5.4.2. Atmospheric Characterization

While the equilibrium temperature of TOI-4364 b is too high to support life, TOI-4364 b is a viable candidate for atmospheric characterization through transmission and emission spectroscopy. With a transit depth of 1.8 ppt, a short orbital period, and the system’s close proximity to Earth, this planet offers a unique opportunity for detailed follow-up observations.

The two panels in [Figure 9](#) illustrate the TSM and ESM values associated with TOI-4364 b (calculations discussed in §5.3) compared to confirmed exoplanets with similar radii in the NASA Exoplanet Archive.⁸ We only illustrate confirmed transiting exoplanets with reliable radii.

With reasonably strong TSM and ESM values, particularly among the population of young planets with well-constrained ages, TOI-4364 b is a compelling candidate for detailed atmospheric characterization. This system has the potential to offer insights into atmospheric retention and planet formation theories in young planetary systems.

Noting its position at the upper edge of the radius valley, this planet could serve as a benchmark to test theories of atmospheric escape, investigating the relevant processes and timescales driving atmospheric loss. Valuable avenues to explore hydrodynamic escape and atmospheric mass loss include transit investigations of atomic hydrogen ($\text{Ly}\alpha$) ([Vidal-Madjar et al. 2003](#)) and metastable helium ($\lambda = 10, 830 \text{ \AA}$) absorption.

6. SUMMARY

In this study, we identified and characterized TOI-4364 b — a transiting mini-Neptune orbiting an M dwarf member of the Hyades cluster. This young planet is located on the upper edge of the radius valley. With a measured radius of $2.01^{+0.10}_{-0.08} R_{\oplus}$ and a relatively short orbital period, the TOI-4364 b likely has an inflated atmosphere due to its young age and high internal entropy.

The discovery of TOI-4364 b adds to our growing census of planetary systems orbiting young M dwarfs. As a cluster member, this newly-detected world benefits from a well-constrained stellar environment, enabling precise age estimates and meaningful comparisons with other

⁸ <https://exoplanetarchive.ipac.caltech.edu/>

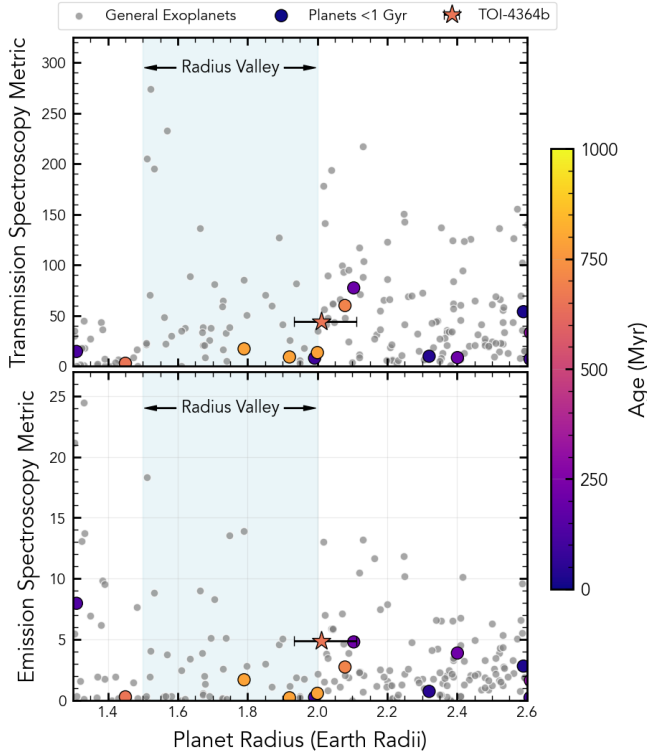


Figure 9. TSM (Top Panel) and ESM (Bottom Panel) values as a function of planet radius for TOI-4364 b (star), the population of confirmed exoplanets (grey circles), and young planets with well-constrained ages (< 1 Gyr, larger circles). The blue shaded region indicates the location of the radius valley as in [Fulton et al. \(2017b\)](#).

exoplanets in similar stages of evolution. This context is crucial for understanding how planetary properties change over time under consistent stellar conditions.

TOI-4364 b’s position near the upper edge of the radius valley offers a valuable case for studying the transition between gas-rich mini-Neptunes and rocky planets. Follow-up RV measurements are essential for determining the planet’s mass, which will help to distinguish between a gas-rich envelope and a rocky, core-dominated planet, shedding light on the processes that shape planets in this size range.

While the TSM and ESM values for this system are modest when compared to the best candidates, they are high when compared to the population of young confirmed exoplanets.

Further, the location of this M dwarf companion at the edge of the radius valley makes it a particularly compelling candidate for atmospheric characterization. TOI-4364 b is well-positioned for spectroscopic and outgassing observations, offering the potential to study its atmospheric composition and evolution. In conclusion, TOI-4364 b represents an important addition to the study of exoplanetary systems orbiting young M dwarfs. The system characteristics offer a promising opportunity

to advance our understanding of planetary atmospheres and evolutionary pathways.

ACKNOWLEDGMENTS

We are thankful for our helpful conversations with Anne Dattilo. MSF gratefully acknowledges the generous support provided by NASA through Hubble Fellowship grant HST-HF2-51493.001-A awarded by the Space Telescope Science Institute, which is operated by the Association of Universities for Research in Astronomy, Inc., for NASA, under the contract NAS 5-26555. AWM was supported by grants from the NSF CAREER program (AST-2143763) and NASA’s exoplanet research program (XRP 80NSSC21K0393). This paper includes data collected by the *TESS* mission, which are publicly available from the Mikulski Archive for Space Telescopes (MAST). Funding for the *TESS* mission is provided by NASA’s Science Mission Directorate. All the *TESS* data used in this paper can be found in MAST: [10.17909/e64q-zy94](https://mast.stsci.edu/portal/#doc/summary?query=10.17909/e64q-zy94). This research has made use of the Exoplanet Follow-up Observation Program (ExoFOP; DOI: 10.26134/ExoFOP5) website, which is operated by the California Institute of Technology, under contract with the National Aeronautics and Space Administration under the Exoplanet Exploration Program. Some of the Observations in the paper made use of the High-Resolution Imaging instruments ‘Alopeke and Zorro’. ‘Alopeke and Zorro were funded by the NASA Exoplanet Exploration Program and built at the NASA Ames Research Center by Steve B. Howell, Nic Scott, Elliott P. Horch, and Emmett Quigley. ‘Alopeke was mounted on the Gemini North, telescope Zorro was mounted on Gemini South telescope, both a part of the international Gemini Observatory, a program of NSF NOIRLab, which is managed by the Association of Universities for Research in Astronomy (AURA) under a cooperative agreement with the U.S. National Science Foundation on behalf of the Gemini Observatory partnership: the U.S. National Science Foundation (United States), National Research Council (Canada), Agencia Nacional de Investigación y Desarrollo (Chile), Ministerio de Ciencia, Tecnología e Innovación (Argentina), Ministério da Ciência, Tecnologia, Inovações e Comunicações (Brazil), and Korea Astronomy and Space Science Institute (Republic of Korea). This work has made use of data from the European Space Agency (ESA) mission *Gaia*,⁹ processed by the *Gaia* Data Processing and Analysis Consortium (DPAC).¹⁰ This research has made use of the VizieR catalogue access tool, CDS, Strasbourg, France. The original description of the VizieR service was published in A&AS 143, 23. We acknowledge the use of public TOI Release data from pipelines at the *TESS* Science Office and the *TESS* Science Processing Operations Center. Resources supporting this work were provided by the NASA High-End Computing (HEC) Program through the NASA Advanced Supercomputing (NAS) Division at Ames Research Center for the production of the SPOC data products.

This publication makes use of data products from the Two Micron All Sky Survey, which is a joint project of the University of Massachusetts and the Infrared Processing and Analysis Center/California Institute of Technology, funded by the National Aeronautics and Space Administration and the National Science Foundation. This work makes use of observations from the LCOGT network. Part of the LCOGT telescope time was granted by NOIRLab through the Mid-Scale Innovations Program (MSIP). MSIP is funded by NSF. Based in part on observations obtained at the Southern Astrophysical Research (SOAR) telescope, which is a joint project of the Ministério da Ciência, Tecnologia e Inovações (MCTI/LNA) do Brasil, the US National Science Foundation’s NOIRLab, the University of North Carolina at Chapel Hill (UNC), and Michigan State University (MSU). Funding for the *TESS* mission is provided by NASA’s Science Mission Directorate. The postdoctoral fellowship of KB is funded by F.R.S.-FNRS grant T.0109.20 and by the Francqui Foundation. KAC and SNQ acknowledge support from the *TESS* mission via subaward s3449 from MIT.

Facilities: *TESS*, *Gaia* DR3 (Gaia Collaboration et al. 2021b); Mikulski Archive for Space Telescopes (Marston et al. 2018); Wide-field Infrared Survey Explorer (*WISE*); LCOGT 1m (Sinistro); LCOGT 1m (NRES); Gemini: Gillett, South; Very Large Telescope; Southern Astrophysical Research (SOAR) Telescope

Software: *AstroImageJ* (Collins et al. 2017), *astroquery* (Ginsburg et al. 2019), *BANZAI* (McCully et al. 2018b), *batman* (Kreidberg 2015), *dustmaps* (Green 2018), *edmc* (Vanderburg 2021), *EXOFASTv2* (Eastman et al. 2013), *Lightkurve* (Lightkurve Collaboration et al. 2018), *matplotlib* (Hunter 2007), *PAdova* and *TRieste Stellar Evolution Code* (Bressan et al. 2012), *PyAstronomy* (Czesla et al. 2019), *starrotate* (Angus & Garcia Soto 2023), *TRICERATOPS* (Giacalone et al. 2021), *TESSCUT* (Brasseur et al. 2019), *Vplanet* (Barnes et al. 2020)

REFERENCES

- Adams, F. C., & Laughlin, G. 2006, *ApJ*, 649, 1004, doi: [10.1086/506145](https://doi.org/10.1086/506145)
- Angus, R., & Garcia Soto, A. 2023, `agarciasoto18/starrotate`: Alternate Starrotate for Paper, v1.1.1, Zenodo, Zenodo, doi: [10.5281/zenodo.7697238](https://doi.org/10.5281/zenodo.7697238)
- Baraffe, I., Homeier, D., Allard, F., & Chabrier, G. 2015, *A&A*, 577, A42, doi: [10.1051/0004-6361/201425481](https://doi.org/10.1051/0004-6361/201425481)
- Barnes, R., Luger, R., Deitrick, R., et al. 2020, *PASP*, 132, 024502, doi: [10.1088/1538-3873/ab3ce8](https://doi.org/10.1088/1538-3873/ab3ce8)
- Brandeker, A., & Cataldi, G. 2019, *Astronomy and Astrophysics*, 621, doi: [10.1051/0004-6361/201834321](https://doi.org/10.1051/0004-6361/201834321)
- Brandner, W., Calissendorff, P., & Kopytova, T. 2023, *Monthly Notices of the Royal Astronomical Society*, 518, doi: [10.1093/mnras/stac2247](https://doi.org/10.1093/mnras/stac2247)
- Brasseur, C. E., Phillip, C., Fleming, S. W., Mullally, S. E., & White, R. L. 2019, `Astrocut`: Tools for creating cutouts of TESS images, *Astronomy Source Code Library*, record ascl:1905.007. <http://ascl.net/1905.007>
- Bressan, A., Marigo, P., Girardi, L., et al. 2012, *Monthly Notices of the Royal Astronomical Society*, 427, doi: [10.1111/j.1365-2966.2012.21948.x](https://doi.org/10.1111/j.1365-2966.2012.21948.x)
- Bressan, A., Marigo, P., Girardi, L., et al. 2012, *MNRAS*, 427, 127, doi: [10.1111/j.1365-2966.2012.21948.x](https://doi.org/10.1111/j.1365-2966.2012.21948.x)
- Brown, T. M., Baliber, N., Bianco, F. B., et al. 2013, *PASP*, 125, 1031, doi: [10.1086/673168](https://doi.org/10.1086/673168)
- Buchhave, L. A., Bakos, G. A., Hartman, J. D., et al. 2010, *Astrophysical Journal*, 720, doi: [10.1088/0004-637X/720/2/1118](https://doi.org/10.1088/0004-637X/720/2/1118)
- Burn, R., Mordasini, C., Mishra, L., et al. 2024, *Nature Astronomy*, 8, doi: [10.1038/s41550-023-02183-7](https://doi.org/10.1038/s41550-023-02183-7)
- Chambers, J. E., & Wetherill, G. W. 1998, *Icarus*, 136, 304, doi: [10.1006/icar.1998.6007](https://doi.org/10.1006/icar.1998.6007)
- Chen, J., & Kipping, D. 2017, *The Astrophysical Journal*, 834, doi: [10.3847/1538-4357/834/1/17](https://doi.org/10.3847/1538-4357/834/1/17)
- Ciardi, D. R., Beichman, C. A., Horch, E. P., & Howell, S. B. 2015, *Astrophysical Journal*, 805, doi: [10.1088/0004-637X/805/1/16](https://doi.org/10.1088/0004-637X/805/1/16)
- Ciardi, D. R., Crossfield, I. J. M., Feinstein, A. D., et al. 2018, *The Astronomical Journal*, 155, doi: [10.3847/1538-3881/aa9921](https://doi.org/10.3847/1538-3881/aa9921)
- Collins, K. A., Kielkopf, J. F., Stassun, K. G., & Hessman, F. V. 2017, *The Astronomical Journal*, 153, 77, doi: [10.3847/1538-3881/153/2/77](https://doi.org/10.3847/1538-3881/153/2/77)
- Collins, K. A., Kielkopf, J. F., Stassun, K. G., & Hessman, F. V. 2017, *AJ*, 153, 77, doi: [10.3847/1538-3881/153/2/77](https://doi.org/10.3847/1538-3881/153/2/77)
- Cowan, N. B., & Agol, E. 2011, *Astrophysical Journal*, 726, doi: [10.1088/0004-637X/726/2/82](https://doi.org/10.1088/0004-637X/726/2/82)
- Curtis, J. L., Agüeros, M. A., Douglas, S. T., & Meibom, S. 2019, *The Astrophysical Journal*, 879, doi: [10.3847/1538-4357/ab2393](https://doi.org/10.3847/1538-4357/ab2393)
- Cutri, R. M., & et al. 2012, *VizieR Online Data Catalog: WISE All-Sky Data Release (Cutri+ 2012)*, *VizieR On-line Data Catalog: II/311*. Originally published in: 2012wise.rept....1C
- Cutri, R. M., Skrutskie, M. F., van Dyk, S., et al. 2003, *2MASS All Sky Catalog of point sources*.
- Czesla, S., Schröter, S., Schneider, C. P., et al. 2019, *PyA: Python astronomy-related packages*. <http://ascl.net/1906.010>
- Dorn, C., Noack, L., & Rozel, A. B. 2018, *Astronomy and Astrophysics*, 614, doi: [10.1051/0004-6361/201731513](https://doi.org/10.1051/0004-6361/201731513)
- Douglas, S. T., Agüeros, M. A., Covey, K. R., & Kraus, A. 2017, *ApJ*, 842, 83, doi: [10.3847/1538-4357/aa6e52](https://doi.org/10.3847/1538-4357/aa6e52)
- Douglas, S. T., Agüeros, M. A., Covey, K. R., et al. 2014, *Astrophysical Journal*, 795, doi: [10.1088/0004-637X/795/2/161](https://doi.org/10.1088/0004-637X/795/2/161)
- Eastman, J., Gaudi, B. S., & Agol, E. 2013, *Publications of the Astronomical Society of the Pacific*, 125, doi: [10.1086/669497](https://doi.org/10.1086/669497)
- Eastman, J. D., Rodriguez, J. E., Agol, E., et al. 2019, *arXiv e-prints*, arXiv:1907.09480, doi: [10.48550/arXiv.1907.09480](https://doi.org/10.48550/arXiv.1907.09480)
- Erkaev, N. V., Kulikov, Y. N., Lammer, H., et al. 2007, *A&A*, 472, 329, doi: [10.1051/0004-6361:20066929](https://doi.org/10.1051/0004-6361:20066929)
- Fűrész, G. 2008, PhD thesis, University of Szeged
- Freund, S., Robrade, J., Schneider, P. C., & Schmitt, J. H. 2020, *Astronomy and Astrophysics*, 640, doi: [10.1051/0004-6361/201937304](https://doi.org/10.1051/0004-6361/201937304)
- Fulton, B. J., Petigura, E. A., Howard, A. W., et al. 2017a, *AJ*, 154, 109, doi: [10.3847/1538-3881/aa80eb](https://doi.org/10.3847/1538-3881/aa80eb)
- . 2017b, *AJ*, 154, 109, doi: [10.3847/1538-3881/aa80eb](https://doi.org/10.3847/1538-3881/aa80eb)
- Furlan, E., & Howell, S. B. 2017, *The Astronomical Journal*, 154, doi: [10.3847/1538-3881/aa7b70](https://doi.org/10.3847/1538-3881/aa7b70)
- . 2020, *The Astrophysical Journal*, 898, doi: [10.3847/1538-4357/ab9c9c](https://doi.org/10.3847/1538-4357/ab9c9c)
- Gaia Collaboration, Prusti, T., de Bruijne, J. H. J., et al. 2016, *A&A*, 595, A1, doi: [10.1051/0004-6361/201629272](https://doi.org/10.1051/0004-6361/201629272)
- Gaia Collaboration, Brown, A. G. A., Vallenari, A., et al. 2021a, *A&A*, 649, A1, doi: [10.1051/0004-6361/202039657](https://doi.org/10.1051/0004-6361/202039657)
- . 2021b, *A&A*, 649, A1, doi: [10.1051/0004-6361/202039657](https://doi.org/10.1051/0004-6361/202039657)
- Gelman, A., & Rubin, D. B. 1992, *Statistical Science*, 7, doi: [10.1214/ss/1177011136](https://doi.org/10.1214/ss/1177011136)
- Giacalone, S., Dressing, C. D., Jensen, E. L. N., et al. 2021, *The Astronomical Journal*, 161, doi: [10.3847/1538-3881/abc6af](https://doi.org/10.3847/1538-3881/abc6af)

- Ginsburg, A., Sipőcz, B. M., Brasseur, C. E., et al. 2019, *AJ*, 157, 98, doi: [10.3847/1538-3881/aafc33](https://doi.org/10.3847/1538-3881/aafc33)
- Ginzburg, S., Schlichting, H. E., & Sari, R. 2018, *MNRAS*, 476, 759, doi: [10.1093/mnras/sty290](https://doi.org/10.1093/mnras/sty290)
- Gladman, B., Quinn, D. D., Nicholson, P., & Rand, R. 1996, *Icarus*, 122, 166, doi: [10.1006/icar.1996.0117](https://doi.org/10.1006/icar.1996.0117)
- Goldreich, P., & Soter, S. 1966, *Icarus*, 5, 375, doi: [10.1016/0019-1035\(66\)90051-0](https://doi.org/10.1016/0019-1035(66)90051-0)
- Gossage, S., Conroy, C., Dotter, A., et al. 2018, *The Astrophysical Journal*, 863, doi: [10.3847/1538-4357/aad0a0](https://doi.org/10.3847/1538-4357/aad0a0)
- Gossage, S., Kalogera, V., & Sun, M. 2023, *The Astrophysical Journal*, 950, doi: [10.3847/1538-4357/acc86e](https://doi.org/10.3847/1538-4357/acc86e)
- Green, G. 2018, *The Journal of Open Source Software*, 3, 695, doi: [10.21105/joss.00695](https://doi.org/10.21105/joss.00695)
- Green, G. M., Schlafly, E., Zucker, C., Speagle, J. S., & Finkbeiner, D. 2019, *The Astrophysical Journal*, 887, doi: [10.3847/1538-4357/ab5362](https://doi.org/10.3847/1538-4357/ab5362)
- Green, G. M., Schlafly, E. F., Finkbeiner, D. P., et al. 2015, *Astrophysical Journal*, 810, doi: [10.1088/0004-637X/810/1/25](https://doi.org/10.1088/0004-637X/810/1/25)
- Griessmeier, J. M., Stadelmann, A., Penz, T., et al. 2004, *Astronomy and Astrophysics*, 425, doi: [10.1051/0004-6361:20035684](https://doi.org/10.1051/0004-6361:20035684)
- Hippke, M., & Heller, R. 2019, *A&A*, 623, A39, doi: [10.1051/0004-6361/201834672](https://doi.org/10.1051/0004-6361/201834672)
- Howell, S. B., Everett, M. E., Sherry, W., Horch, E., & Ciardi, D. R. 2011, *Astronomical Journal*, 142, doi: [10.1088/0004-6256/142/1/19](https://doi.org/10.1088/0004-6256/142/1/19)
- Hunter, J. D. 2007, *Computing in Science and Engineering*, 9, 90, doi: [10.1109/MCSE.2007.55](https://doi.org/10.1109/MCSE.2007.55)
- Jenkins, J. M. 2002, *ApJ*, 575, 493, doi: [10.1086/341136](https://doi.org/10.1086/341136)
- Jenkins, J. M., Tenenbaum, P., Seader, S., et al. 2020, *Kepler Data Processing Handbook: Transiting Planet Search*, Kepler Science Document KSCI-19081-003, id. 9. Edited by Jon M. Jenkins.
- Jenkins, J. M., Chandrasekaran, H., McCauliff, S. D., et al. 2010, in *Society of Photo-Optical Instrumentation Engineers (SPIE) Conference Series*, Vol. 7740, *Software and Cyberinfrastructure for Astronomy*, ed. N. M. Radziwill & A. Bridger, 77400D, doi: [10.1117/12.856764](https://doi.org/10.1117/12.856764)
- Jenkins, J. M., Twicken, J. D., McCauliff, S., et al. 2016, in *Proc. SPIE*, Vol. 9913, *Software and Cyberinfrastructure for Astronomy IV*, 99133E, doi: [10.1117/12.2233418](https://doi.org/10.1117/12.2233418)
- Johnson, D. R. H., & Soderblom, D. R. 1987, *AJ*, 93, 864, doi: [10.1086/114370](https://doi.org/10.1086/114370)
- Kempton, E. M., Bean, J. L., Louie, D. R., et al. 2018, *Publications of the Astronomical Society of the Pacific*, 130, doi: [10.1088/1538-3873/aadf6f](https://doi.org/10.1088/1538-3873/aadf6f)
- Kipping, D. 2023, *Monthly Notices of the Royal Astronomical Society*, 523, doi: [10.1093/mnras/stad1492](https://doi.org/10.1093/mnras/stad1492)
- Kite, E. S., Manga, M., & Gaidos, E. 2009, *Astrophysical Journal*, 700, doi: [10.1088/0004-637X/700/2/1732](https://doi.org/10.1088/0004-637X/700/2/1732)
- Kovács, G., Zucker, S., & Mazeh, T. 2002, *A&A*, 391, 369, doi: [10.1051/0004-6361:20020802](https://doi.org/10.1051/0004-6361:20020802)
- Kreidberg, L. 2015, *PASP*, 127, 1161, doi: [10.1086/683602](https://doi.org/10.1086/683602)
- Li, J., Tenenbaum, P., Twicken, J. D., et al. 2019, *PASP*, 131, 024506, doi: [10.1088/1538-3873/aaf44d](https://doi.org/10.1088/1538-3873/aaf44d)
- Lightkurve Collaboration, Cardoso, J. V. d. M., Hedges, C., et al. 2018, *Lightkurve: Kepler and TESS time series analysis in Python*, *Astrophysics Source Code Library*. <http://ascl.net/1812.013>
- Lodieu, N., Smart, R. L., Pérez-Garrido, A., & Silvotti, R. 2019, *Astronomy and Astrophysics*, 623, doi: [10.1051/0004-6361/201834045](https://doi.org/10.1051/0004-6361/201834045)
- Lomb, N. R. 1976, *Ap&SS*, 39, 447, doi: [10.1007/BF00648343](https://doi.org/10.1007/BF00648343)
- Long, L., Bi, S., Zhang, J., et al. 2023, *The Astrophysical Journal Supplement Series*, 268, doi: [10.3847/1538-4365/ace5af](https://doi.org/10.3847/1538-4365/ace5af)
- Lopez, E. D., & Fortney, J. J. 2014, *ApJ*, 792, 1, doi: [10.1088/0004-637X/792/1/1](https://doi.org/10.1088/0004-637X/792/1/1)
- Lopez, E. D., Fortney, J. J., & Miller, N. 2012, *ApJ*, 761, 59, doi: [10.1088/0004-637X/761/1/59](https://doi.org/10.1088/0004-637X/761/1/59)
- Luger, R., & Barnes, R. 2015, *Astrobiology*, 15, 119, doi: [10.1089/ast.2014.1231](https://doi.org/10.1089/ast.2014.1231)
- Mann, A. W., Newton, E. R., Rizzuto, A. C., et al. 2016, *AJ*, 152, 61, doi: [10.3847/0004-6256/152/3/61](https://doi.org/10.3847/0004-6256/152/3/61)
- Mann, A. W., Vanderburg, A., Rizzuto, A. C., et al. 2018, *The Astronomical Journal*, 155, doi: [10.3847/1538-3881/aa9791](https://doi.org/10.3847/1538-3881/aa9791)
- Marston, A., Hargis, J., Levay, K., et al. 2018, in *Society of Photo-Optical Instrumentation Engineers (SPIE) Conference Series*, Vol. 10704, *Observatory Operations: Strategies, Processes, and Systems VII*, 1070413, doi: [10.1117/12.2311973](https://doi.org/10.1117/12.2311973)
- McCully, C., Volgenau, N. H., Harbeck, D.-R., et al. 2018a, in *Society of Photo-Optical Instrumentation Engineers (SPIE) Conference Series*, Vol. 10707, *Software and Cyberinfrastructure for Astronomy V*, ed. J. C. Guzman & J. Ibsen, 107070K, doi: [10.1117/12.2314340](https://doi.org/10.1117/12.2314340)
- McCully, C., Volgenau, N. H., Harbeck, D.-R., et al. 2018b, in *Society of Photo-Optical Instrumentation Engineers (SPIE) Conference Series*, Vol. 10707, *Software and Cyberinfrastructure for Astronomy V*, ed. J. C. Guzman & J. Ibsen, 107070K, doi: [10.1117/12.2314340](https://doi.org/10.1117/12.2314340)
- Mestel, L. 1968, *Monthly Notices of the Royal Astronomical Society*, 140, doi: [10.1093/mnras/140.2.177](https://doi.org/10.1093/mnras/140.2.177)

- Mignon, L., Meunier, N., Delfosse, X., et al. 2023, *Astronomy and Astrophysics*, 675, doi: [10.1051/0004-6361/202244249](https://doi.org/10.1051/0004-6361/202244249)
- Morbidelli, A., Lunine, J. I., O'Brien, D. P., Raymond, S. N., & Walsh, K. J. 2012, *Annual Review of Earth and Planetary Sciences*, 40, 251, doi: [10.1146/annurev-earth-042711-105319](https://doi.org/10.1146/annurev-earth-042711-105319)
- Morris, R. L., Twicken, J. D., Smith, J. C., et al. 2020, *Kepler Data Processing Handbook: Photometric Analysis*, Kepler Science Document KSCI-19081-003, id. 6. Edited by Jon M. Jenkins.
- Newton, E. R., Mann, A. W., Tofflemire, B. M., et al. 2019, *ApJL*, 880, L17, doi: [10.3847/2041-8213/ab2988](https://doi.org/10.3847/2041-8213/ab2988)
- Oh, S., & Evans, N. W. 2020, *Monthly Notices of the Royal Astronomical Society*, 498, doi: [10.1093/mnras/staa2381](https://doi.org/10.1093/mnras/staa2381)
- Owen, J. E., & Wu, Y. 2017, *The Astrophysical Journal*, 847, 29, doi: [10.3847/1538-4357/aa890a](https://doi.org/10.3847/1538-4357/aa890a)
- Pepe, F., Cristiani, S., Rebolo, R., et al. 2021, *A&A*, 645, A96, doi: [10.1051/0004-6361/202038306](https://doi.org/10.1051/0004-6361/202038306)
- Pierrehumbert, R. T., & Hammond, M. 2019, *Atmospheric Circulation of Tide-Locked Exoplanets*, doi: [10.1146/annurev-fluid-010518-040516](https://doi.org/10.1146/annurev-fluid-010518-040516)
- Quinn, S. N., White, R. J., Latham, D. W., et al. 2014, *Astrophysical Journal*, 787, doi: [10.1088/0004-637X/787/1/27](https://doi.org/10.1088/0004-637X/787/1/27)
- Rebull, L. M., Stauffer, J. R., Bouvier, J., et al. 2016, *AJ*, 152, 113, doi: [10.3847/0004-6256/152/5/113](https://doi.org/10.3847/0004-6256/152/5/113)
- Ricker, G. R., Winn, J. N., Vanderspek, R., et al. 2015, *Journal of Astronomical Telescopes, Instruments, and Systems*, 1, 014003, doi: [10.1117/1.JATIS.1.1.014003](https://doi.org/10.1117/1.JATIS.1.1.014003)
- Rogers, L. A. 2015, *ApJ*, 801, 41, doi: [10.1088/0004-637X/801/1/41](https://doi.org/10.1088/0004-637X/801/1/41)
- Röser, S., Schilbach, E., & Goldman, B. 2019, *Astronomy and Astrophysics*, 621, doi: [10.1051/0004-6361/201834608](https://doi.org/10.1051/0004-6361/201834608)
- Sato, B., Izumiura, H., Toyota, E., et al. 2007, *The Astrophysical Journal*, 661, doi: [10.1086/513503](https://doi.org/10.1086/513503)
- Scargle, J. D. 1982, *ApJ*, 263, 835, doi: [10.1086/160554](https://doi.org/10.1086/160554)
- Scott, N. J., Howell, S. B., Gnilka, C. L., et al. 2021, *Frontiers in Astronomy and Space Sciences*, 8, doi: [10.3389/fspas.2021.716560](https://doi.org/10.3389/fspas.2021.716560)
- Skumanich, A. 1972, *The Astrophysical Journal*, 171, doi: [10.1086/151310](https://doi.org/10.1086/151310)
- Smith, J. C., Stumpe, M. C., Van Cleve, J. E., et al. 2012, *PASP*, 124, 1000, doi: [10.1086/667697](https://doi.org/10.1086/667697)
- Stellingwerf, R. F. 1978, *The Astrophysical Journal*, 224, doi: [10.1086/156444](https://doi.org/10.1086/156444)
- Stumpe, M. C., Smith, J. C., Catanzarite, J. H., et al. 2014, *PASP*, 126, 100, doi: [10.1086/674989](https://doi.org/10.1086/674989)
- Stumpe, M. C., Smith, J. C., Van Cleve, J. E., et al. 2012, *PASP*, 124, 985, doi: [10.1086/667698](https://doi.org/10.1086/667698)
- Szentgyorgyi, A. H., & Furész, G. 2007, in *Revista Mexicana de Astronomia y Astrofisica: Serie de Conferencias*, Vol. 28
- Taberero, H. M., Montes, D., & Hernández, J. I. G. 2012, *Astronomy and Astrophysics*, 547, doi: [10.1051/0004-6361/201117506](https://doi.org/10.1051/0004-6361/201117506)
- Tittlemore, W. C., & Wisdom, J. 1990, *Icarus*, 85, 394, doi: [10.1016/0019-1035\(90\)90125-S](https://doi.org/10.1016/0019-1035(90)90125-S)
- Tokovinin, A. 2018, *Publications of the Astronomical Society of the Pacific*, 130, doi: [10.1088/1538-3873/aaa7d9](https://doi.org/10.1088/1538-3873/aaa7d9)
- Twicken, J. D., Clarke, B. D., Bryson, S. T., et al. 2010, in *Society of Photo-Optical Instrumentation Engineers (SPIE) Conference Series*, Vol. 7740, *Software and Cyberinfrastructure for Astronomy*, ed. N. M. Radziwill & A. Bridger, 774023, doi: [10.1117/12.856790](https://doi.org/10.1117/12.856790)
- Twicken, J. D., Catanzarite, J. H., Clarke, B. D., et al. 2018, *PASP*, 130, 064502, doi: [10.1088/1538-3873/aab694](https://doi.org/10.1088/1538-3873/aab694)
- Vanderburg, A. 2021, *avanderburg/edmcmc: v1.0.0*, v1.0.0, Zenodo, Zenodo, doi: [10.5281/zenodo.5599854](https://doi.org/10.5281/zenodo.5599854)
- Vanderburg, A., Mann, A. W., Rizzuto, A., et al. 2018, *The Astronomical Journal*, 156, doi: [10.3847/1538-3881/aac894](https://doi.org/10.3847/1538-3881/aac894)
- Vanderburg, A., Huang, C. X., Rodriguez, J. E., et al. 2019, *ApJL*, 881, L19, doi: [10.3847/2041-8213/ab322d](https://doi.org/10.3847/2041-8213/ab322d)
- Vidal-Madjar, A., Lecavelier des Etangs, A., Désert, J. M., et al. 2003, *Nature*, 422, 143, doi: [10.1038/nature01448](https://doi.org/10.1038/nature01448)
- Watson, A. J., Donahue, T. M., & Walker, J. C. G. 1981, *Icarus*, 48, 150, doi: [10.1016/0019-1035\(81\)90101-9](https://doi.org/10.1016/0019-1035(81)90101-9)
- Winters, J. G., Henry, T. J., Jao, W.-C., et al. 2019, *The Astronomical Journal*, 157, doi: [10.3847/1538-3881/ab05dc](https://doi.org/10.3847/1538-3881/ab05dc)
- Wright, E. L., Eisenhardt, P. R. M., Mainzer, A. K., et al. 2010, *AJ*, 140, 1868, doi: [10.1088/0004-6256/140/6/1868](https://doi.org/10.1088/0004-6256/140/6/1868)
- Zacharias, N., Finch, C. T., Girard, T. M., et al. 2013, *Astronomical Journal*, 145, doi: [10.1088/0004-6256/145/2/44](https://doi.org/10.1088/0004-6256/145/2/44)
- Ziegler, C., Tokovinin, A., Briceño, C., et al. 2020, *AJ*, 159, 19, doi: [10.3847/1538-3881/ab55e9](https://doi.org/10.3847/1538-3881/ab55e9)